PROCEEDINGS OF SPIE

Analytical and finite element analysis tool for nonlinear membrane antenna modeling for astronomical applications

Palisoc, Arthur, Pardoen, Gerard, Takashima, Yuzuru, Chandra, Aman, Sirsi, Siddharta, et al.

SPIE.

Analytical and finite element analysis tool for nonlinear membrane antenna modeling for astronomical applications

Arthur L. Palisoc[1,a], Gerard Pardoen[b], Yuzuru Takashima[c], Aman Chandra[d], Siddhartha Sirsi[c], Heejoo Choi[c], Daewook Kim[c], Henry Quach[c], Jonathan W. Arenberg[e], Christopher Walker[c,f]

[a]L'Garde, Inc.,15181 Woodlawn Ave, Tustin CA, USA 92780-6487; [b]Environmental & Civil Engineering Dept., University of California, Irvine, CA 92697; [c]Wyant College of Optical Sciences, University of Arizona, 1630 University Blvd, Tucson, AZ 85721-0094; [d]Aerospace & Mech. Engr Dept., University of Arizona 1130 N. Mountain Ave, Tucson, AZ; [e]Northrop Grumman, One Space Park, Redondo Beach California 90278; [f]Dept. of Astronomy and Steward Observatory, University of Arizona, 933 N. Cherry Ave, Tucson, AZ 85721

ABSTRACT

The uninflated shape configurations of parabolic and spherical membrane mirrors were calculated by solving the inverse problem, i.e., given the design inflation pressure, the membrane material and geometric properties, what must be the initial uninflated shape such that on inflation to the design pressure, the exact desired surface of revolution is obtained. The resulting first order nonlinear differential equation was numerically integrated using the boundary conditions. The initial uninflated shape was then subjected to a forward transformation using FAIM, a proprietary geometric nonlinear membrane finite element code. FAIM has been validated against exact analytical solutions for both small and extremely large deformations that are up to eight orders of magnitude larger compared with the starting undeflected shape. Simulations reveal that to fabricate a very accurate and precise inflated membrane mirror relative to the design parameters, one must not only accurately measure and input the moduli in both meridional and hoop directions but an accurately measured Poisson's ratio as well. The code was used to guide the membrane mirror design. For very small aperture diameters, the initial uninflated shape may be fabricated by thermo-forming the membrane. For aperture diameters exceeding one meter however, the membrane mirror is built with discrete gores that are joined together with tapes at the seams. This provided the impetus to write a companion computer code FLATE, to calculate the gore shapes using a slight modification of the solution to the inverse transformation equation to account for the presence of the seam tapes. After the gores were determined, the resulting final inflated shape was calculated and verified using FAIM. Sensitivity analyses can now be carried out to determine the resulting surface shape as a function of the different sources of error: gore width, gore length, perimeter attachment uncertainties, thermal effects, variation of material properties over the membrane continuum and inflation pressure changes. The code has been shown to be more robust than equivalent commercial analytical packages in so far as *membrane*, *cable* and *space-frame* element combinations are concerned. In particular, the analytical and finite element codes were used in the preliminary assessment of a membrane optic for the OASIS Mission (Orbiting Astronomical Satellite for Investigating Stellar Systems) [1]. The OASIS is a 20-meter class space observatory operating at high spectral resolution in the terahertz frequencies. Over its nominal 2-year mission it will probe conditions and search for biogenic molecules on hundreds of protoplanetary disks and other solar system objects.

Keywords: Finite element analysis, inflatable membrane mirror, geometric nonlinear, inverse shape problem solution

1. INTRODUCTION

For telescopes and antennas, aperture is everything – whether they are terrestrial or space-based. Very large aperture telescopes can easily be constructed and erected on the ground but the same cannot be said if the telescope is intended to be put in space. The cost of putting a telescope in orbit is orders of magnitude more expensive and if conventional telescope

---

[1] art_palisoc@lgarde.com; phone 1 714 259-0771 x 228; fax 1 714 259-7822; www.lgarde.com

technology is used, the aperture size gets limited by packaged volume, i.e., the packaged unit must fit within the fairing of currently available rocket boosters. The James Webb Space Telescope (JWST) that is due for launch in November 2021 is 6 ½ meters in diameter. Once on operation, the JWST becomes the largest aperture telescope operating in the infrared, overtaking the 3.5-meter Herschel. The JWST will undoubtedly provide exciting science information never before seen but just imagine how much more science one can collect and be surprised with, with an aperture ten times larger. The desire to have a launchable large diameter antenna/telescope provided the impetus to create an analytical tool capable of determining accurately what design parameters are needed to achieve requisite surface accuracies coupled with the ability for a telescope primary to be stowable into a small volume. And once on orbit, the antenna/telescope deploys to full aperture with non- or minimally degraded performance. The resulting analytical tool developed is a nonlinear finite element code for membranes. There are commercial nonlinear codes in the market, but they are very expensive and for the problems analyzed in this paper, the codes found it challenging to converge to the right solution. The commercial codes needed some "assistance" to converge.

The primary candidate for a lightweight and packageable telescope mirror is a space hazard resistant polyimide membrane coated with a few thousand angstroms of aluminum. The telescope mirror is constructed using the mirror-membrane formed into a surface of revolution, e.g., paraboloid or sphere. Inflation is used to maintain the surface shape configuration where the reflector and canopy form a lenticular configuration as shown in Fig. 1. A stiff toroidal ring is used to constrain the inflated lenticular and prevent it from collapsing inward. One other advantage of an inflatable system is its inherent high damping characteristics. Typical structural damping coefficients are between 5% and 20%.[2]


| (A) | (B) |
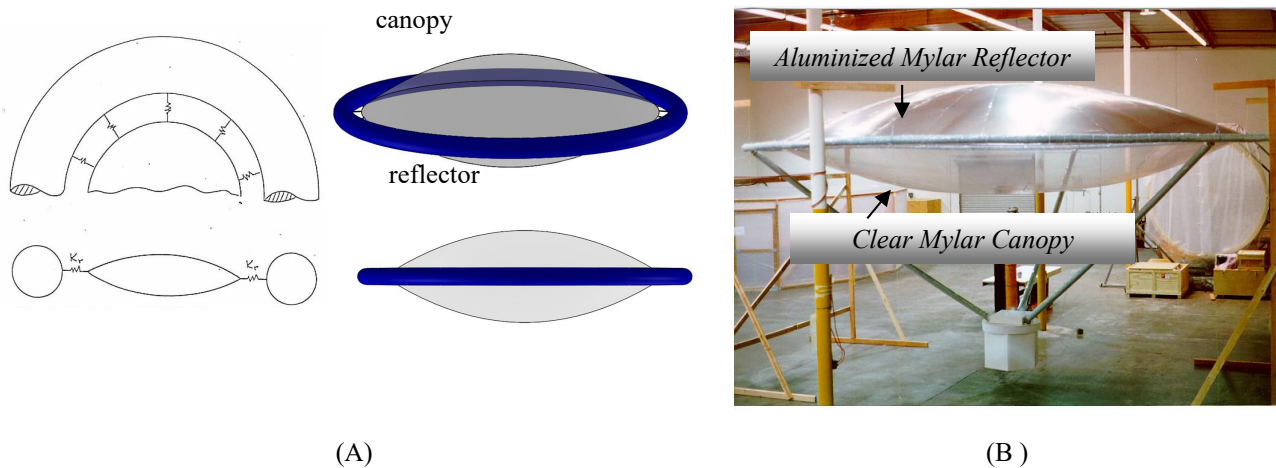
Figure 1. (A) Inflatable lenticular surface of revolution. In the analysis, the toroidal ring may be replaced by a spring boundary condition, K_r. (B) A 7-meter diameter inflatable paraboloid lenticular engineering model built by L'Garde. The torus and three struts were made of inflatable gel-rigidizable material.

Figure 2A shows the 14-meter diameter Inflatable Antenna Experiment (IAE) [2] undergoing ground testing and Fig. 2B is a 3-meter diameter sector of the same reflector. Figure 2C shows the IAE, minutes after launch from the Space Shuttle STS-77 mission in May 1996 – the earth is in the background.

One of the major concerns with inflatables in space is the effect of impact with natural and man-made debris particles. Although most of the particles, especially micrometeoroids, are very small, with diameters on the order of microns, their velocities can be up to 20 km/sec and even higher – the energy of impact is immense. These pose a serious threat especially to inflatable space structures. The detailed analysis of the effect of natural and man-made debris is not the subject of this paper but suffice it to say that the inflatable membrane mirrors for space-based telescopes can be designed such that it only takes very little pressure to smooth out the surface. As an example, the 14-meter diameter Inflatable Antenna Experiment (IAE) reflector was pressurized to only *1/33,000th* of an atmosphere and that was more than sufficient to render the reflector surface very specular, Fig. 2. The reason for this is the low membrane thickness used coupled with a large effective radius: 28 meters for the IAE. It is therefore noted that the absolute inflation pressure needed to stress a thin film to a value to make for a very smooth and mirror-like surface is small especially for surfaces of revolution with very large radii as is the case for most space applications. The pressure is so low that the rate of inflatant loss due to micrometeoroid punctures

can be affordably replaced by carrying makeup gas on board. [3,4] The OASIS 20-meter diameter reflector pressure is only 1/30,000[th] of an atmosphere and can be attributed to its large surface radius of 50m - the inflatant gas is in the free-molecular flow regime.[5]

| (A) | (B) | (C) |
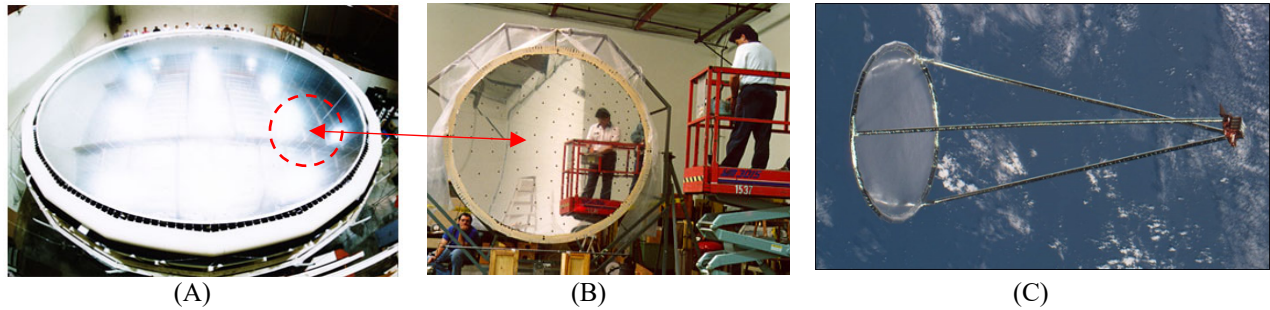
Figure 2. (A) 14-meter diameter Inflatable Antenna Experiment (IAE) reflector undergoing ground surface accuracy tests at the L'Garde Tustin California facility – fabrication team in the background, (B) 3-meter diameter sector of the IAE, (C) Photographed from the Space Shuttle: the 14-meter IAE on-orbit, jettisoned from the Space Shuttle STS-77 in May 1996. The earth is in the background.

2. SOLVING THE INVERSE PROBLEM

In this section a method to solve the *inverse problem* is outlined: *given the final desired surface shape, inflation pressure, material and geometric properties of the membrane, what must be the initial uninflated shape so that on inflation to the specified pressure, the initial shape configuration transforms to the desired surface of revolution.* This is a statement of the *inverse problem*.

2.1 Paraboloid [6]

Consider the two states of a thin-walled shell membrane described schematically in Fig. 3. An axisymmetric shell of uniform thickness, whose coordinates are distinguished by a *prime,* describes the uninflated membrane. When inflated, the membrane is transformed into an axisymmetric paraboloid defined by $z = r^2/4F$. In this geometric formulation, F refers to the focal length of the parabola. In the forward transformation of the uninflated axisymmetric shell to the inflated paraboloidal shell, infinitesimal arc elements in the circumferential and meridional directions are stretched from their uninflated lengths dc' and ds' to corresponding inflated lengths dc and ds respectively. The strains in the circumferential and meridional directions are given by

$$d\epsilon_c = \frac{dc - dc'}{dc'} \tag{1a}$$
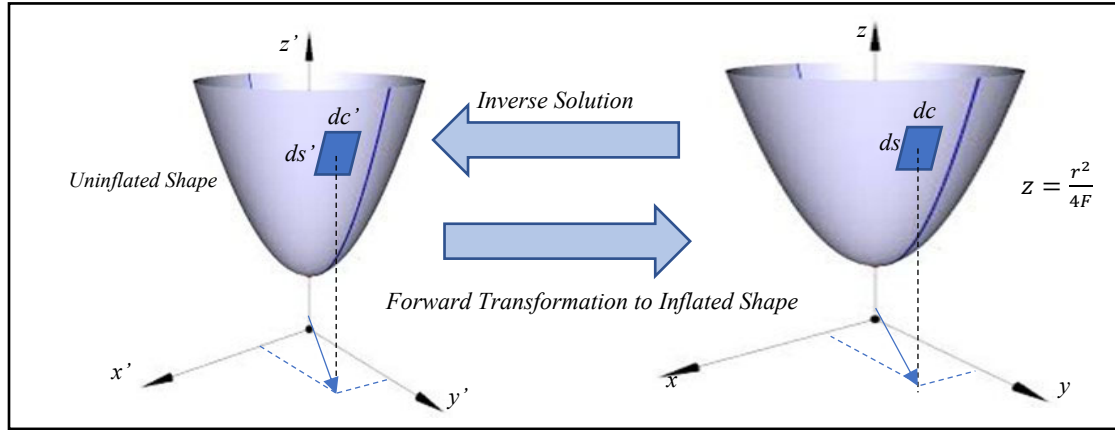
and

$$d\epsilon_m = \frac{ds - ds'}{ds'}. \tag{1b}$$

In Eqs. (1) the ϵ_i are the membrane strains. For an orthotropic material ν_{cm} and ν_{mc} represent the *Poisson ratios* and obey the following relationship:

$$\frac{\nu_{cm}}{\nu_{mc}} = \frac{E_c}{E_m} \tag{2}$$

where the E_i are the elastic moduli in the circumferential and meridional directions. The large stress-strain relation is used to account for large deformations and the more general expression using tensor relationships is used:

$$S_c = \frac{E_c}{(1 - \nu_{cm}\nu_{mc})} \left\{ \frac{1 + \epsilon_c}{1 + \epsilon_m} \right\} \left[\left\{ \epsilon_c + \frac{\epsilon_c^2}{2} \right\} + \nu_{mc} \left\{ \epsilon_m + \frac{\epsilon_m^2}{2} \right\} \right] \tag{3a}$$

$$S_m = \frac{E_m}{(1-\nu_{cm}\nu_{mc})}\left\{\frac{1+\epsilon_m}{1+\epsilon_c}\right\}\left[\left\{\epsilon_m + \frac{\epsilon_m^2}{2}\right\} + \nu_{cm}\left\{\epsilon_c + \frac{\epsilon_c^2}{2}\right\}\right] \tag{3b}$$

Figure 3. Shell membrane profile before and after pressurization showing differential elements of the surface.

When the static equilibrium of the paraboloidal membrane is considered, the two principal stresses in the shell membrane may be expressed in terms of the inflation pressure p, the thickness t and the focal length F as follows:

$$S_c = \frac{pF}{t}\frac{1+2(r/2F)^2}{\sqrt{1+(r/2F)^2}} \tag{4a}$$

$$S_m = \frac{pF}{t}\sqrt{1+(r/2F)^2} \tag{4b}$$

The arc lengths in Eqs. (1) may be expressed in terms of the membrane geometry as

$$dc = rd\theta \tag{5a}$$

$$dc' = r'd\theta \tag{5b}$$

$$ds = \sqrt{dr^2 + dz^2} \tag{5c}$$

$$ds' = \sqrt{dr'^2 + dz'^2} \tag{5d}$$

Recall the geometric equation of the paraboloid:

$$z = r^2/4F \tag{6a}$$

$$dz/dr = r/2F \tag{6b}$$

Substituting Eqs. (5) into Eqs. (1) and using Eqs. (6) yields

$$\epsilon_c = \frac{r}{r'} - 1 \tag{7a}$$

$$\epsilon_m = \sqrt{\frac{1+(r/2F)^2}{(dr'/dr)^2+(dz'/dr)^2}} - 1 \qquad (7b)$$

The set of six equations, Eqs. (1) through (5) and (7) have been developed for six unknowns: the two principal stresses S_c, S_m, the two principal strains ϵ_c, ϵ_m, and the coordinates r' and z', defining the shape of the uninflated membrane in terms of r, the radial coordinate of the inflated paraboloid. The solution of these equations defines the precise shape of the uninflated membrane needed to achieve a pressurized paraboloid exactly defined by $z = r^2/4F$.

2.2 Sphere [6]

The inverse problem for the sphere of radius R is solved in a similar manner with Eqs. (4) replaced by

$$S_c = \frac{pR}{2t} \qquad (8a)$$

$$S_m = \frac{pR}{2t} \qquad (8b)$$

noting that for an inflated thin membrane sphere, $S_c = S_m$. The analogs of Eqs. (6) and (7b) for the sphere are, respectively

$$z = R\left(1 - \sqrt{1 - (r/R)^2}\right) \qquad (9a)$$

$$\frac{dz}{dr} = \frac{r/R}{\sqrt{1-(r/R)^2}} \qquad (9b)$$

and

$$\epsilon_m = \sqrt{\frac{1}{[(dr'/dr)^2+(dz'/dr)^2][1-(r/R)^2]}} - 1 \qquad (10)$$

The six equations in the six unknowns are then solved for the uninflated spherical membrane surface shape. These equations have been incorporated into the FLATE code – Section 2.3.

2.3 The FLATE code

The equations in Sections 2.1 and 2.2 were solved and a computer code FLATE was written to include the gore flat pattern calculation given the number of gores desired. The use of *doubler* material; i.e. tape, to join gores at the seams have also been accounted for in the calculation of the flat pattern. A special case of direct sun-staring condition has also been included. FLATE can also handle orthotropic materials where the moduli in the machine and transverse directions are different. In fact, this is the case for both Mylar and Kapton where not only are the moduli different in the perpendicular directions but when one measures the modulus as a function of orientation in the material, one gets an ellipse, where the distance from the center to the periphery of the ellipse is the value of the modulus along that orientation. Mylar and Kapton are anisotropic with Mylar exhibiting higher anisotropic behavior than Kapton.[7]

Figure 4 shows a gore flat pattern. The FLATE code has an added feature where the *optimum pressure* may be calculated iteratively as a function of number of gores. This pressure is defined as the pressure that stretches the thicker seam to the same final length as the center of the gore. Because the optimum pressure may be high for a given application, it cannot always practically be used, hence a numerical step-by-step procedure was created to determine the outer edge perimeter gore edge shape when an arbitrary pressure is desired. [8]
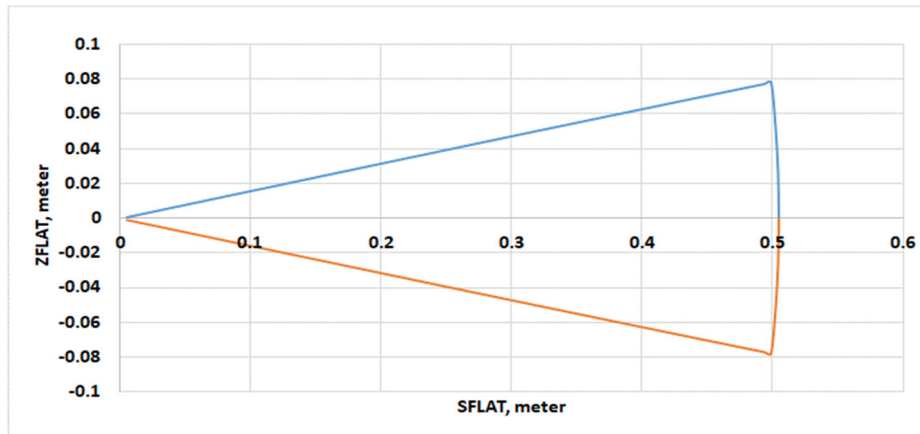
Figure 4. Example gore flat pattern calculated by FLATE for a 1m diameter *F/D=1* paraboloid antenna with 20 gores. The flat pattern fits the initial uninflated configuration. The slight curvature of the side edges depends on the number of gores used. *SFlat* and *ZFlat* are terminologies used by the FLATE code.

3. FORWARD TRANSFORMATION: FINITE ELEMENT ANALYZER FOR INFLATABLE MEMBRANES – THE FAIM CODE [9, 10, 11, 12]

FAIM is a general-purpose finite element code for determining the stresses and deformations of inflatable shell membranes due to internal pressure. It uses a numerically intensive, iterative procedure to solve the nonlinear equilibrium equations to a user-specified desired degree of accuracy. A restart capability is provided to achieve higher levels of accuracy than those obtained from a previous analysis. It is a geometric nonlinear finite element calculator. A pre- and post- processor for FAIM was coded based on Femap [13]. The stiffness and mass matrix generated by the code may be input to an eigenvalue solver to calculate modes and natural frequencies of the material continuum.

3.1 FAIM Element Library

The elements in the FAIM library are shown in Fig. 5. A 6-node isoparametric triangle, an 8-node isoparametric quadrilateral and a 3-node tension only cable element are the basic elements of the code. More recently, a fourth element was added. It is the 2-node space frame element. A conscious decision was made early on to discard the computational advantage of the 3-node triangle and the 4-node quadrilateral shell elements since these elements were deemed too crude to provide the requisite deformation information. A 3-node triangle for instance can only approximate the smooth surface of an inflatable parabolic shell surface with a collection of flat, triangular facets. These facets, each of which has a constant slope are simply not adequate when one needs to determine the surface slope throughout the continuum. In contrast, the 8-node quad and 6-node triangle do not have these limitations. A 3-node tension only cable element was included because of the need to include the effect of the stiffer, thicker seams. The thicker seam area can be modeled by quads and triangles, but the seam width is much smaller than the gore width. Modeling the seams this way would result in a prohibitively large number of elements.

FAIM was initially designed to analyze linear elastic material and a geometrically nonlinear deformation behavior. A nonlinear material capability has since been added although for most inflatable applications for space, geometrical nonlinear behavior dominates, i.e., the strains involved are small, but the geometric deflections are orders of magnitude greater than the material thickness. It is also noted that the code now includes anisotropic shell membrane material capability. The need to consider geometric nonlinear behavior of the membrane is obvious when one considers that linear theory assumes that the deformation normal to the element surface is only a fraction of the thickness whereas deformations of inflatable membrane shells are several orders of magnitude greater than the membrane thickness.
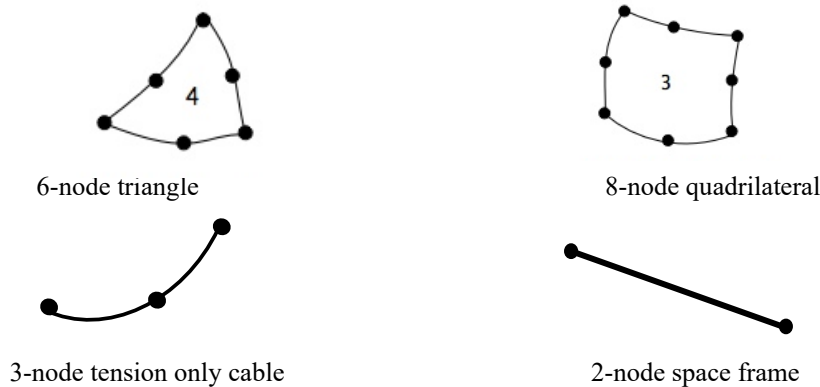
Figure 5. Elements in the FAIM library.

3.2 A Multitude of Loadings and Boundary Conditions

The loadings available in a FAIM analysis are (a) follower pressure, (b) concentrated nodal forces, (c) 3D arbitrary body force accelerations and (d) nodal or element temperatures. Several enhancements have been added to increase the analysis capabilities as well as its computational efficiency. A "spring boundary condition" capability was coded in anticipation of the need to characterize the outer radius mounting surface of the surface of revolution to a flexible rather than an infinitely rigid support as shown in Fig. 6. In Fig. 6, the toroidal ring is replaced by springs characterized by spring constant

$$K_r = \frac{EA}{R^2}$$

Where E is the torus material modulus, A is the cross-sectional area of the torus and R is the major torus radius.
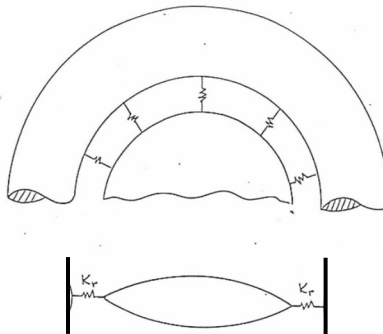
Figure 6. "Spring Boundary Condition". The flexible toroidal support ring is replaced by "springs" of constant K_r.

Another feature available in FAIM is what is called a "skew" boundary condition. Referring to the axisymmetric finite element model depicted in Fig. 7 we note that this model required the x-y-z displacements at the outer radius to be zero as well as specifying that the circumferential displacements along the radial edges be zero due to symmetry conditions. The symmetry required on the circumferential displacement necessitated an implementation of the "skew" boundary condition. A skew boundary condition means a node is restrained to move along a plane not parallel to the global x-y, y-z and x-z planes.

Both a zero and non-zero displacement boundary conditions are available. The non-zero displacement boundary condition can be used to model "pre-stress"; e.g., the outer edge nodes of the gore are displaced (stretch) to their final inflated locations.

The significant computational efficiency enhancements to FAIM include a new solution strategy for solving the large number of simultaneous equations as well as a "restart capability". There are three significant contributions to the coefficient matrix of these equations: (1) elastic terms, (2) geometric terms, and (3) pressure terms. Whereas the first two lead to a symmetric coefficient matrix, the third leads to a skew symmetric. The combination of these three effects leads to an unsymmetric matrix. FAIM now has two simultaneous equation algorithms for solving the equilibrium equation of a shell membrane model: (a) symmetric, banded coefficient matrix and (b) unsymmetric, banded coefficient matrix solution. Both solution strategies are implemented "in-core". This has an obvious advantage and disadvantage at the same time. Because it is an in-core solution, it is very fast. However, for the same reason, it can analyze only a problem small enough that will fit in main memory. With current advanced operating systems, *memory paging* is used if the RAM is not large enough to accommodate the entire matrix "in-core" but at the expense of increased CPU execution time.

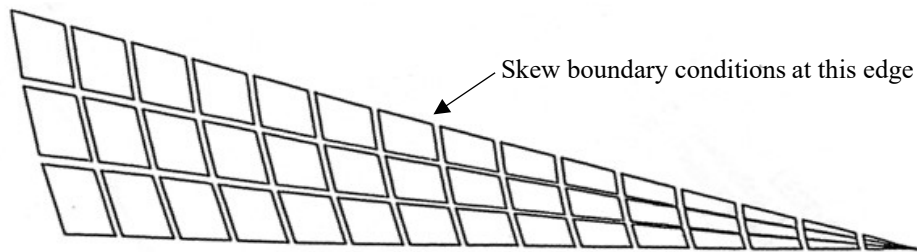Skew boundary conditions at this edge

Figure 7. Axisymmetric finite element FAIM model of a shell of revolution.

The symmetric solution strategy takes some numerical shortcuts to achieve efficiency. One then may initially ignore the resulting minor contributions of the pressure term that results in an unsymmetric matrix and assume that the resulting matrix is symmetric. This shortcut significantly reduces the execution time by a factor of 5 to 10 and requires only about half as much storage. Once a satisfactory equilibrium state has been achieved to a desired degree of accuracy with the symmetric albeit slightly inaccurate coefficient matrix, one can repeatedly solve the simultaneous equations with the proper unsymmetric coefficient matrix using the "restart capability".

After creating the finite element model with all its nodes and element connectivity, including the material and geometric properties, the entire FAIM input text script is fed into a companion *node renumbering* computer program, REN. REN uses the GPS algorithm [14] to minimize the matrix bandwidth.

## 3.3 Validation of the FAIM Code – the Inverse and Hencky [15] Problems

This section details three analytical and one experimental validation of the FAIM calculations: (a) "inflation" of the uninflated shape (solution to the inverse problem), (b) deflection of a flat circular membrane (Hencky Problem), (c) temperature-loaded flat circular membrane, and (d) measurement of the deflections of a pre-stressed 1 meter diameter membrane.

3.4 Forward Loading -evolution of the uninflated configuration towards the ideal paraboloid shape

An exact solution has been derived for the inverse problems for the seamless paraboloid and sphere in Section 2. In this section we carry out a forward transformation using FAIM. The analytically derived initial uninflated shapes of a paraboloid for three values of the Poisson's ratio were "inflated" using FAIM and the results are shown in Fig. 8.

In Fig. 8, the results are expressed in terms of the dimensionless parameters $(Z/2F)$ and $(r/2F)$ where F is the paraboloid focal length, z is the vertical displacement and r is the radial distance from the vertex. The inflation pressure used is $pF/Et=1$ and for typical membrane materials, this translates to a very high pressure. For example, for a membrane with $E=3.45\ GPa$ and using $t = 12.7\ microns$ and $F=5m$, $p=8.8\ kPa$, the resulting film stress is *3.45 GPa (500,000 psi)*. This is only a theoretical exercise to show the large deflection case. This is indeed an extremely high inflation pressure and results in very large (geometrically nonlinear) deflections as can be seen in Fig. 8. The results in Figure 8 show that for the three different initial uninflated shapes corresponding to three different values of Poisson's ratio, FAIM converges to

the analytical result. The results also indicate that the Poisson's ratio is very important. In practice, to obtain the correct initial uninflated shape, the Poisson's ratio and elastic modulus must be measured accurately.
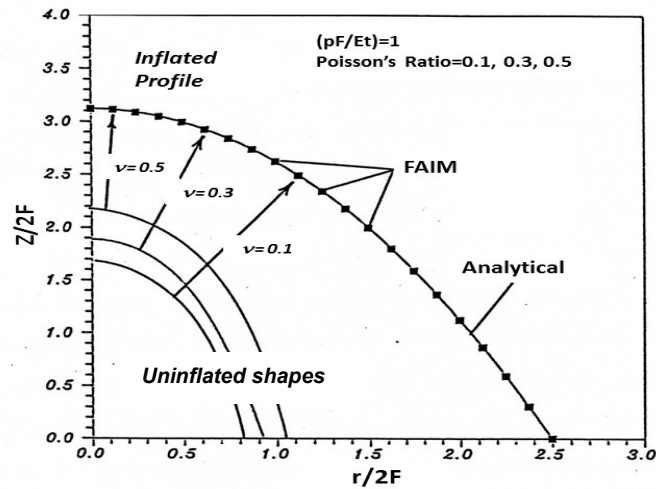
Figure 8. Comparison of analytical and FAIM results: the analytical solution is that of the inverse problem for a seamless paraboloid.

3.5 Deflection of flat circular membrane – the Hencky [15] problem

A classic series-solution for the stress and deformation of a pressurized circular membrane may be derived [15, 16]. The z-deflection of the flat membrane as a function of pressure is given by [16]

$$w(\rho) = q^{1/3} \sum_0^\infty a_{2n}(1 - \rho^{2n+2}) \tag{11}$$

where,

ρ: dimensionless radial coordinate and

q: dimensionless loading parameter $= \dfrac{pa}{Eh}$; a =radius, p=pressure, E=modulus, h= membrane thickness.

Tables 1 and 2 list the evaluated coefficients taken from ref. 13.

Table 1. Coefficients of the Series Solution for the flat membrane deflection.

| Coefficients	Value
a_0	0.543419194
a_2	0.043602350
a_4	0.007774497
a_6	0.001715457
a_8	0.000420438
a_{10}	0.000109772
a_{12}	2.99016E-05
a_{14}	8.39701E-06
a_{16}	2.41279E-06
a_{18}	7.05823E-07
a_{20}	2.09468E-07

Table 2. Table of coefficient b_o as a function of Poisson Ratio. a_o is a function of b_o.

Poisson's Ratio	b_o
0.2	1.6827
0.3	1.7244
0.4	1.7769
0.5	1.8402

Equation (11) with the coefficients given in Tables 1 and 2 were used to calculate the deflection of an initially flat circular membrane. The membrane properties are listed in Table 3. The results of the FAIM calculation expressed in non-dimensional units are shown in Fig. 9. The actual dimensions are obtained by multiplying the horizontal and vertical axes by the radius. The solid circles in the curve are FAIM results.

Table 3. Flat circular membrane parameters.

Parameter	Value	Unit
Diameter	20	meter
Elastic Modulus	2.78	GPa
Membrane thickness	12.7	microns
Pressure	0.0026995	18.6 Pa
Poisson's ratio used	0.1, 0.3, 0.5	-
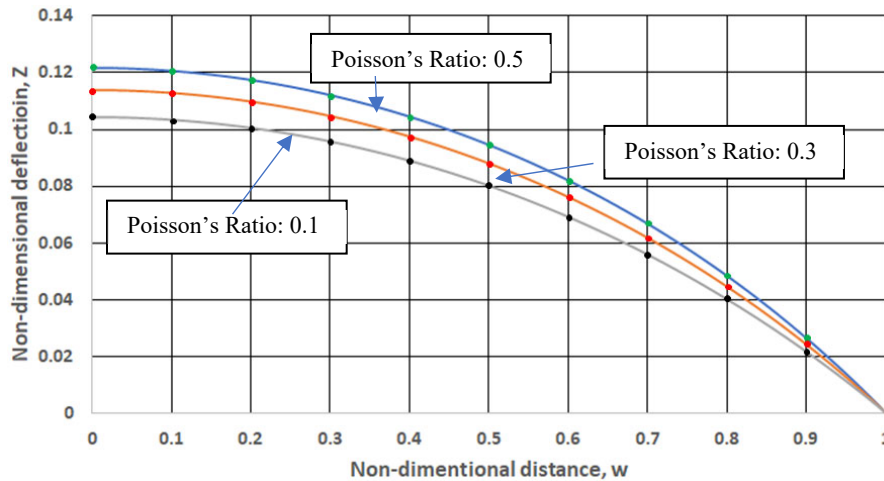
Figure 9. Deflection of initially flat circular membrane under pressure, expressed in non-dimensional units. The circular *centered symbols* are the FAIM results.

The stresses for the flat circular membrane are likewise predicted quite accurately by FAIM.[17]

### 3.5.1 Temperature loading of a flat circular disk [18,19,20,21]

The last analytical validation/verification check of FAIM is comparison of its prediction of the radial deflections and stresses on a flat circular disk subjected to the following temperature loading conditions:

Uniform radial temperature distribution $T_o(r) = T_o$ (12)

Linear radial temperature distribution $T_1 = T_o + (T_R - T_o)\frac{r}{R}$ (13)

Quadratic radial temperature distribution $T_2 = T_o + (T_R - T_o)\left(\frac{r}{R}\right)^2$ (14)

In Eqs. (12) through (14), r is the radial distance from the center, R is the radius of the disk, T_o is the temperature at the center and T_R is the temperature at $r = R$. The results of the runs using FAIM compared with theory [21] are shown in Fig. 10. The solid lines in the figures correspond to the theoretical values. The solid symbols, squares, diamonds, and triangles are FAIM-predicted and correspond to the uniform, linear and quadratic temperature distributions, respectively. The axisymmetric finite element model is shown in Fig. 11. It is a 15-degree slice of the disk.
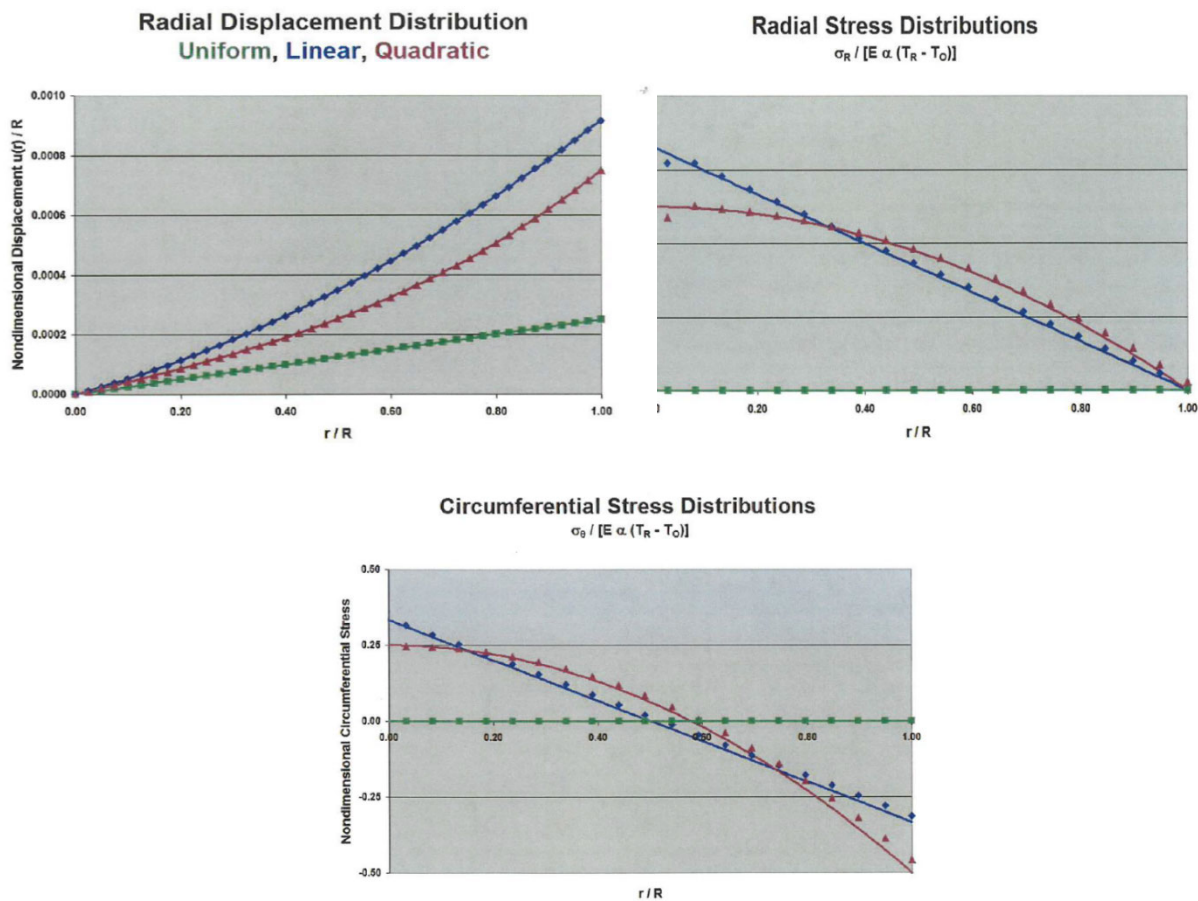
Figure 10. Radial displacements, radial stresses and circumferential stresses on a temperature-loaded membrane disk.
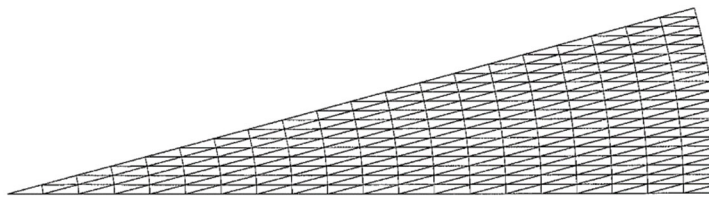

Figure 11. 15-degree axisymmetric slice, 400 triangle element model of the thermally loaded circular disk.

3.6 Comparison with Measurements of a Pre-stressed 1m Flat Circular Membrane

In this section we present the results of the comparison between FAIM and the measurement of the pressurized profile of initially pre-stressed 1 meter diameter Mylar and Kapton membranes. Since it is easier to achieve and control a finite, non-zero initial prestress state in a membrane than an initial zero stress condition, the membranes used in the experiment were given an initial prestress of 345 kPa (50 psi). Table 4 lists the properties of the circular flat membranes measured. The VSTARS photogrammetry system from Geodetic Services, Inc. of Melbourne, Florida was used in the profile measurement.

Table 4. Parameters of the 1.0 Meter Circular Membranes Measured using Photogrammetry.[7]

Parameter	Kapton (Isotropic)	Mylar (Orthotropic -30°)
Thickness	12.7 microns	12.7 microns
Measured Modulus	3.74 GPa	$E_1 = 6.46\ GPa;\ E_2 = 4.47\ GPa$
Poisson's Ratio	0.3	$\nu_{12} = 0.35 \quad \nu_{21} = 0.24$
Diameter	1.0 meter	1.0 meter
Prestress	345 kPa	345 kPa
Pressures used	17.24 and 206.84 Pa	11.7 and 124.1 Pa
Stresses due to pressure	4.39 kPa; 12.2 kPa	4.6 kPa; 27.6 kPa
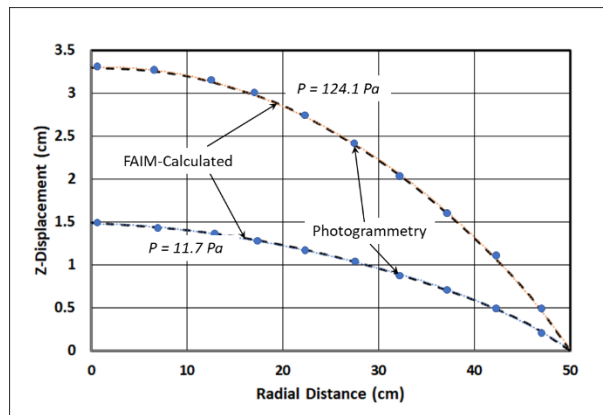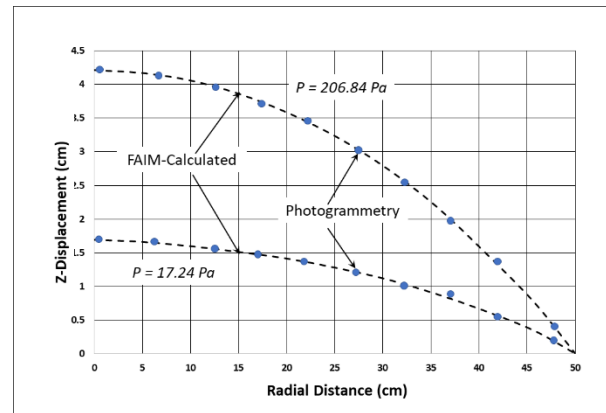
| (A) | (B) |

Figure 12. (A) Measured Mylar profile. (B) Measured Kapton profile. Two inflation pressures used for each. The corresponding stresses are shown in Table 4.

The Young's modulus and Poisson's ratios were measured using a video metrology system. The values shown in Table 4 are average values. While Kapton is isotropic, Mylar is orthotropic with principal material axes approximately 70 degrees from the material machine direction. The results of the measurement are shown in Fig. 12. The predictions by FAIM are superimposed on the same plot. The error bars correspond to the uncertainties in the measurement of the pressure and the nonuniformity of the modulus over the material surface. However, a 10% higher (or lower) modulus value corresponds to only a 3% decrease (or increase) in the vertical deflection of the membrane. For Mylar, the uncertainty in the modulus is +10%/-5% and for Kapton, it is ±6%. Notice the excellent agreement between FAIM and measurements especially for Mylar. The agreement is not as good for Kapton, Fig. 12B but it is still within experimental error. The reason for this is that the Kapton membrane used was not as "flat" as the Mylar. In fact, even after the Kapton was pre-stressed to 345 kPa (50 psi), certain sections of the Kapton showed minor rippling. This is believed to have previously existed in the material as a result of how it was rolled-packaged around its central cardboard cylinder hub. There are other types of Kapton, such

as Kapton E that exhibits far more uniformity than the Kapton HN used. Kapton E was not available during the time of the measurement. The size of the circle symbols in Figure 12 may be taken as the length of the error bars. The VSTARS photogrammetry system used had an accuracy of 1/100,000 of the characteristic size of the article under test. In this case that is *1m/100,000 = 10⁻⁴ m or 0.1 mm*.

3.7 The effect of seams

Figure 13 shows how a real inflatable membrane antenna-reflector is fabricated. Gores, very much like those of an umbrella (see Fig. 4) are bonded together at the seams. The gores are joined together using an overlap or a butt joint seam. Therefore, where the seams are, the material is considerably thicker and stiffer compared with the gore material. It is noted that since the gore pattern is a two-dimensional flat, the initial shape prior to pressurization curves only in the meridional direction and are flat faceted along the circumference. In the inflated state, inflation pressure provides additional curvature along the circumference.

Past measurements of the surface profiles showed that the effect of the seams on surface accuracy was relatively minimal. Surface errors were generally slowly varying across the membrane exhibiting a "*W*" or "*M*" curve as illustrated in Fig. 14. [22] The curve shown in Fig. 14B is a plot of the deviation of the measured surface with the calculated best-fit paraboloid. The vertical axis, *Δz* is the deviation in millimeters. It was found from previous testing that when the membrane included seams, the result was a slight bumpiness in the error profile which retained the "*W*" of "*M*" shape at nearly the same level as without seams. Since the test article tested was fabricated using gores calculated by FLATE (Sect. 2.3), the presence of the seams has been taken into consideration and hence one would expect to not have considerable error contribution from these regions. As will be shown in the following, the use of FAIM shows that the contribution to the error in surface shape is small compared to the observed surface deviations in typical inflatable membrane reflectors. The significance of these findings is that inflatable membrane reflectors can be made inexpensively using seamed construction with no appreciable degradation of surface accuracy when compared to more expensive, monolithic continuous formed membranes.


| (A) | (B) | (C) |
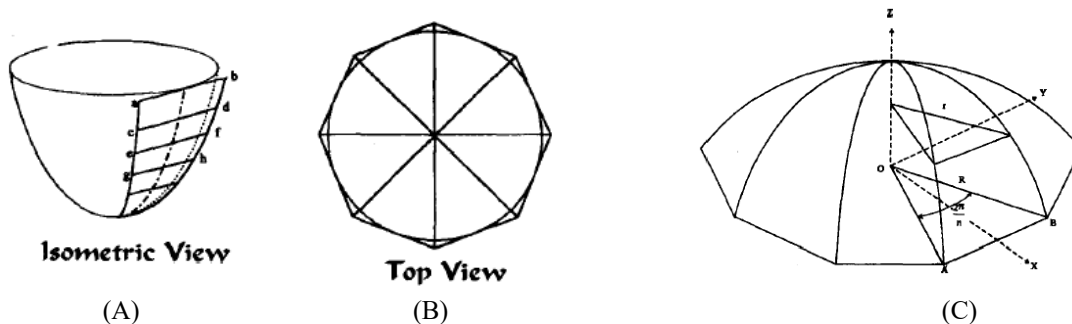
Figure 13. Parabolic antenna reflector geometry for FAIM analysis. (A) The center line of the gore flat pattern is along the ideal uninflated shape of revolution that was calculated by solving the inverse problem. (B) Top view. (C) gores seamed together to form the initial uninflated seamed configuration.

FAIM was used to analytically assess the effect of seams on the rms surface accuracy, and the results published in ref. 22. Three analytical cases with and without seams were examined: (i) deflection of a one-meter diameter six gore, flat circular membrane, (ii) deflection of a one-meter six-gore pre-formed spherical membrane, and (iii) deflection of an axisymmetric 64-gore, 14-meter diameter on-axis parabolic reflector. The resulting deflections for the flat membranes, cases (i) and (ii) were fitted to the Hencky equation, using the following form:

$$z = P_1 + P_2(x^2 + y^2) + P_3(x^2 + y^2)^3 \tag{15}$$

The full circular configuration was used in this particular case and the finite element model is shown in Fig. 15A. For the preformed case, a 1-meter diameter membrane was taken from a sphere of 241.3 cm radius. The material thickness was 12.7 microns. The seam tape was 0.953 cm wide and 12.7 microns thick. The results are shown in Tables 5 and 6.

(A)   (B)
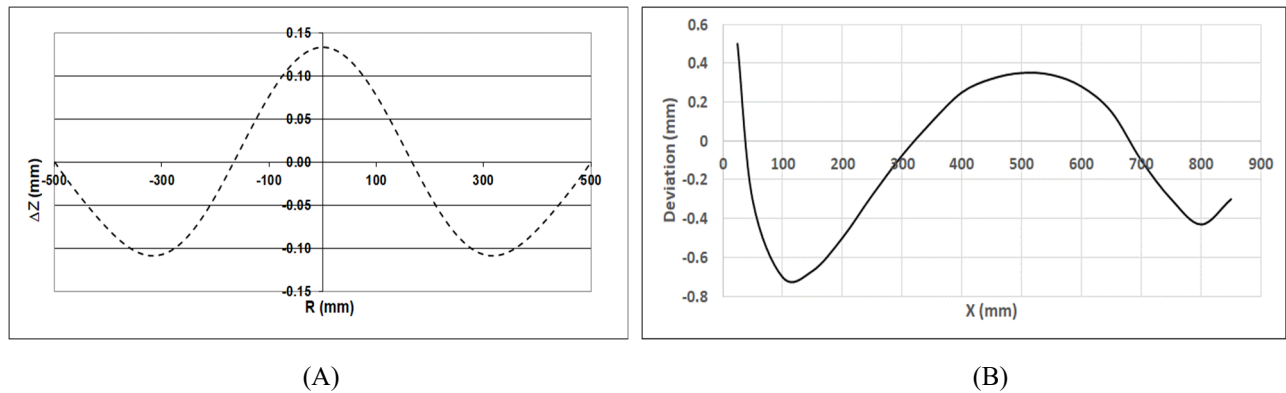
Figure 14. (A) Ideal example of "W" curve deviation from the best fit paraboloid. (B) Actual measured rms deviation from the best-fit paraboloid, for a 1meter diameter aperture [22].

The results in Tables 5 and 6 show that the change in the rms surface accuracy relative to the membrane surface shape is small. As expected, the cable elements (seam tapes) provide some stiffening as expressed by P_1 but the surface accuracy relative to the overall profile remains about the same. Moreover, when precision inflatable structures are designed using flat gores, the effect of the seams must be taken into account, as was in this case in order to get as close to the desired final inflated configuration.

(A)   (B)
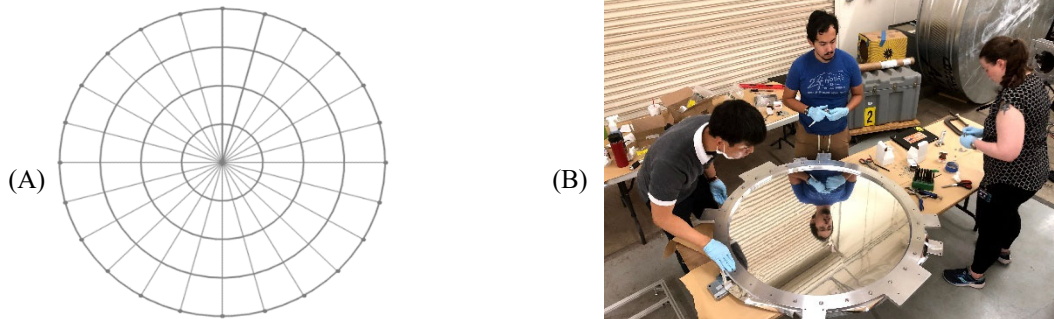
Figure 15. (A) Finite element model of a 1-meter diameter flat circular membrane. (B) A 1m Flat Circular Membrane being mounted on its ring support at the University of Arizona. `

The case shown in Table 6 is that of a 64-gore, 14-meter diameter on-axis inflatable parabolic reflector. The *F/D* ratio is *1.0* and the material used was 6.35 microns thick with a modulus of 3.45 GPa and a Poisson's ratio of 0.3. The surface was fitted to the following (paraboloid) equation:

$$z = z_o + \frac{1}{4F}[(x - x_o)^2 + (y - y_o)^2]$$
(16)

Only the case with seams is shown in Table 6 since we have already seen that FAIM predicts the final inflated shape to a high degree of accuracy even of a highly deformed seamless membrane – Fig. 8. The RMS surface accuracy predicted is 0.11 mm RMS. This is about an order of magnitude lower error than that measured for large reflectors such as the IAE [2]. When designed properly, seamed inflatable reflectors, even the large diameters, can be tailored to be accurate.

Table 5. Parameters [Eq. (15)] for flat circular membrane.

Parameter	Without seam tape	With seam tape
P_1 (cm)	7.3418	7.2128
P_2 (cm^{-1})	-0.00247	-0.00237
P_3 (cm^{-3})	-1.8604 x 10^{-7}	-2.2244 x 10^{-7}
Sum of squares (cm^2)	0.00861	0.0157
RMS Deviation (mm)	0.087	0.117

Table 6. Parameters [Eq. (15)] for pre-formed circular membrane.

Parameter	Without seam tape	With seam tape
P_1 (cm)	245.7668	243.1058
P_2 (cm^{-1})	-0.00289	-0.00279
P_3 (cm^{-3})	-2.2315 x 10^{-7}	-2.4637 x 10^{-7}
Sum of squares (cm^2)	0.01382	0.01991
RMS Deviation (mm)	0.110	0.132

Table 6. Parameters of Eq. (16) for the 14-meter diameter inflatable reflector with seams.

| Parameter	Value with seams
$1/4F$; (m^{-1})	0.1807
x_o; (cm)	13.797
y_o; (cm)	0.732
z_o; (cm)	0.721
RMS Deviation; (mm)	0.110

4. THE OASIS REFLECTOR [1]

4.1 OASIS Reflector Parameters

We next present the FAIM analysis of the preliminary configuration of the primary membrane mirror of the 20-meter aperture diameter OASIS [1] reflector. Table 7 lists the OASIS parameters. The axisymmetric seamless case was analyzed, and the finite element model is similar to that shown in Fig. 11. An artist's concept of the OASIS is shown in Fig. 16. The telescope consists of an inflatable reflector secured to a spacecraft via deployable inflatable-rigidizable struts. A closed loop adaptive optics system continuously measures the reflector's surface and compensates for distortions, using a deformable mirror [1]. The toroidal ring constrains the inflatable lenticular perimeter from collapsing inward due to the reaction in response to the internal pressure. The toroidal ring is made of the same material as the struts. Because all three major components of the telescope – the primary mirror, toroidal ring and struts – are made of inflatable-rigidizable material, the system is very lightweight and stows with very high packaging efficiency.   From preliminary analysis, it is estimated that the packaging volume required is on the order of 1 m^3.

Table 7. OASIS reflector.

| Parameter	Value
Aperture diameter (m)	20
Conic Constant (parabola)	-1
Radius at vertex (m)	50
Focal length (m)	25
Membrane thickness (microns)	12.7
Inflation pressure Pa (atm)	3.5 (3.45 x 10^{-5})
Film stress Pa (atm)	6.895 x 10^6 (68)
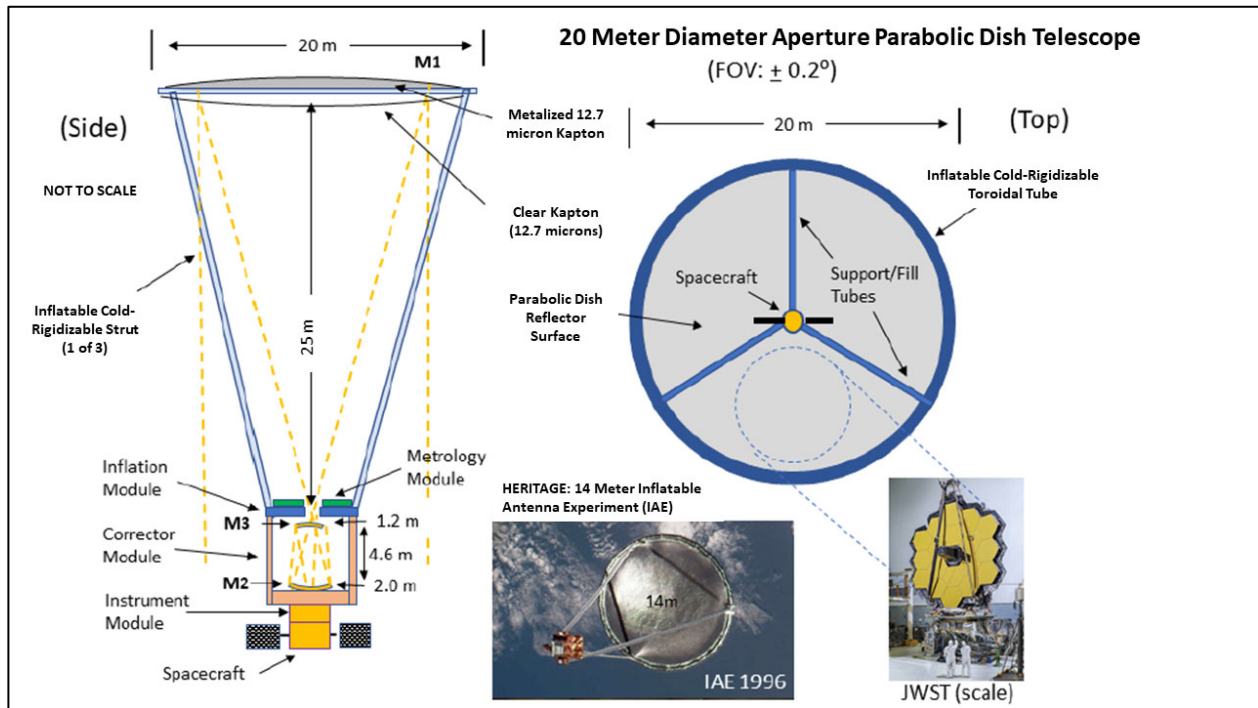
Figure 16. The OASIS inflatable reflector. [1]

4.2 Inflating the OASIS Reflector using FAIM

The OASIS uninflated seamless shape was calculated using the FLATE code (Sect. 2.3) and was used to generate an axisymmetric model. Skew boundary conditions were used along the gore side edge and the nodes at the outer periphery of the uninflated gore shape were displaced to their final locations in the inflated state using FAIM's displacement boundary condition capability. Figure 17 shows the uninflated and final inflated configurations including the direction of the applied pressure. For the inflation pressure used, the inflated and uninflated configurations are very close to each other. Figure 17B is a close up of the radial region starting at 8 meters. The two shapes differ from each other by about 10 centimeters in the RMS sense.

Two other pressure cases were run: ten percent higher and ten percent lower than the nominal value. The finite element results were run through a best-fit parabola calculation and are shown in Table 8. The x_o, y_o and z_o are the translation parameters in the best-fit calculation. There are two other rotation (Euler Angle) parameters, and like the translation parameters, they are small due to the axisymmetric nature of the FAIM finite element model. The *rms* value is relative to the best-fit paraboloid.
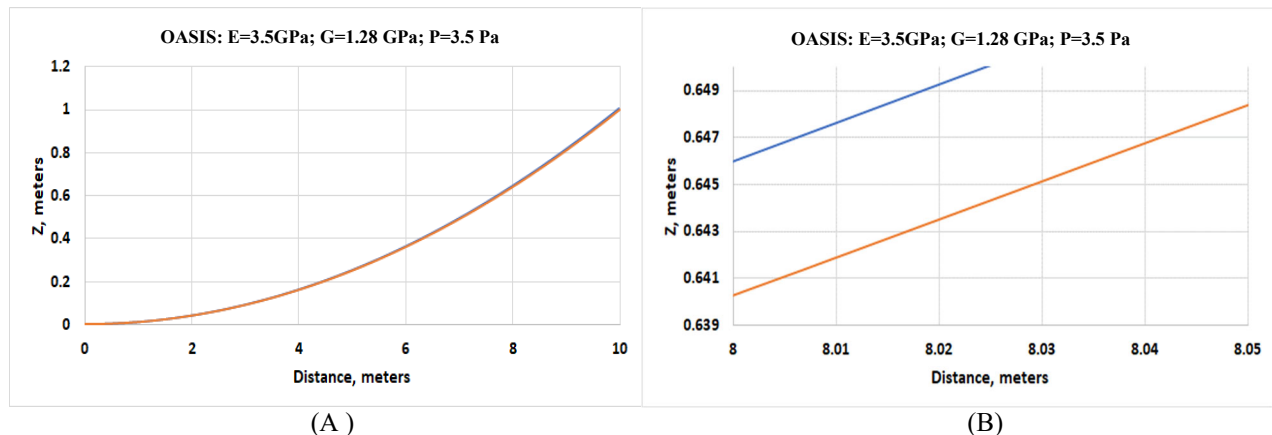
Figure 17. The OASIS reflector. (A) uninflated and final inflated configuration. (B) Closeup near $r = 8$ *meter* region. The uninflated shape is above the inflated shape. Pressurization direction is indicated by the arrow.

Table 8. Results for the OASIS reflector.

Best-fit Parameters	IDEAL	Nominal Pressure	10% Lower Pressure	10% Higher Pressure
Focal Length (m)	25	25.013	25.220	24.810
x_o (cm)	0	2.02 x 10^{-5}	3.07 x 10^{-3}	-6.57 x 10^{-3}
y_o (cm)	0	2.31 x 10^{-4}	-1.82 x 10^{-2}	0.2143
z_o (cm)	0	5.948 x 10^{-2}	1.029	-0.893
rms (mm)	0	0.028	0.718	0.587

Nominal pressure: *3.5 Pa (5.08 x 10^{-4} psi)*; reflector membrane film stress: *6.89 MPa (1,000 psi)*

From Table 8, it is seen that the higher pressure case results in a deeper parabola with a shorter focal length as expected. The lower pressure case turns the surface flatter with the focal length slightly longer than nominal. Again, this is expected. The nominal pressure case exhibits the lowest rms value – it is closest to the desired ideal shape but the rms and the other best-fit parameters although small, did not "FAIM-calculate" to zero. This is due to the fact that the finite element model used a finite number of elements - it is a 3.46-degree axisymmetric slice with 861 nodes and 400 elements. Increasing the nodal and element discretization density should only bring the nominal case result closer to the ideal.

A few more finite element runs can be made to get a good measure of the change in focal length as a function of pressure ($\Delta F / \Delta p$). This will be useful in the optical simulation of the OASIS. Collaboration with Takashima, et al [23] at the University of Arizona and scientists at Northrop-Grumman [4] is on-going and possible enhancements to FAIM may be made to increase its capabilities including facilitated modeling of the continuum with material properties varying with position. The cases shown in Table 8 have been used by Takashima, et al [23] to carry out optics simulation to get a measure of the secondary and tertiary mirror sizes. For even larger reflectors, one must result to using analytics as it will be expensive and difficult to perform the experimental measurements, e.g., finding a large enough thermal vacuum chamber to test a 40m diameter or greater aperture.

4.3 Sensitivity Analyses

The surface accuracy of an inflatable reflector depends on several factors. These include (a) material property uniformity over the surface, (b) gore shape accuracy, (c) seaming accuracy, (d) inflation pressure stability, and (e) temperature change and temperature uniformity of the surface. The probability distribution (Gaussian, Weibull, etc.) of all these sources of

errors can be determined and used in the finite element analyses and the most probable values with corresponding uncertainties used to carry out analytical runs in a limited Monte-Carlo sense, from which an error budget table can be created. Table 9 is the result of analyses carried out on the Large Inflatable Structures (LIS) project [24]. The error budget in Table 9 was to achieve a surface accuracy on the order of a few millimeters RMS on 7m to 15m aperture diameter reflectors. An error budget table similar to Table 9 will be generated for the OASIS project but for sub-millimeter rms surface accuracy.

Table 9. Fabrication Error Budget for Inflatable Antenna Reflector.

Error Source	Budget
Gore Width	$\pm\,0.10$ mm
Gore Seaming	$\pm\,0.05$ mm
Gore Length	$\pm\,0.1$ mm per meter length
Mounting	$\pm\,0.38$ mm
Material non-uniformity	$M_o\;\pm\,0.04M_o$
Temperature at manufacture	$T_o\;\pm\,2\,°C$
Humidity at manufacture	$H_o\;\pm\,5\%\,RH$

On orbit, the main contributor to the overall surface accuracy will be the non-uniform temperature distribution over the reflector surface and inflation pressure stability. The errors introduced for the direct sun-staring case can be eliminated by design - the FLATE code has this capability. It is the off-boresight reflector-to-sun angles that result in large temperature gradients that contribute to surface degradation of a few millimeters rms. The OASIS team is currently evaluating the use of *Novastrat*, a zero-CTE polyimide from Nexolve, Inc. [25]

5. SUMMARY AND CONCLUSIONS

The resulting shape geometry of inflatable membrane reflectors for both initially flat and initially curved surfaces were presented. The use of reliable analytical codes is deemed to be of utmost importance to guide the design. The validity of the codes used was tested against known analytical solutions and experimental measurements. From experience, in so far as membrane and cable elements are concerned the FAIM code has been shown to be robust. Given a set of correct input, loading and boundary conditions, FAIM converges to the correct results. There are commercially available codes that can be used but they are expensive and more often, the user has to have the necessary experience and know-how to coax the code to achieve convergence and to know whether or not the code converged to the correct results. The results of the present study show the feasibility of using inflated membrane shape for space reflector applications approaching the terahertz operating frequency of OASIS.

6. REFERENCES

[1] C. Walker, et al., "Orbiting Astronomical Satellite for Investigating Stellar Systems (OASIS): Following Water from the Interstellar Medium to Oceans", Bulletin of the AAS, vol 51, issue 7, Sept. 2019.

[2] R.E. Freeland, G.D. Bilyeu, G.R. Veal, M.D. Steiner, D.E. Carson, "Large inflatable deployable antenna flight experiment results", Acta Astronautica, vol. 41, Issue 4-10, pp 267-277 (1997).

[3] A.L. Palisoc, "Inflatable Reflector Development Program, Task 3 Report", L'Garde Technical Report, LTR-94-AP-008, May 1994.

[4] J. Arenberg," Environmental Challenges to OASIS's Primary Reflector", This Conference, Proc SPIE, Optics+Photonics, San Diego, California, 1-5 August 2021.

[5] M. Thomas and G. Friese, "Pressurized antennas for space radars", AIAA paper 80-1928, CP, AIAA Sensor Systems for the 80's Conference, Dec. 1980.

[6] G.C. Pardoen, "Orthotropic, Parabolic Shell Membrane Analysis", Technical report submitted to L'Garde, 1992.

[7]   A.L. Palisoc, "Geometry attained by pressurized membranes", Proc SPIE, Space Telescopes and Instruments, pp 747-756, (1998)

[8] A.L. Palisoc, "Procedure for finding the gore ends for reflector gores when the optimum pressure is not used", L'Garde Technical Report, Dec. 1996.

[9] G.H. Powell and Eberhard Haug, "Finite element analysis of nonlinear membrane structures", Structural Engineering and Structural Mechanics, University of California, Berkeley, Feb. 1972

[10] G.H. Powell, "Theory of nonlinear elastic structures", Journal of the Structural Division, ASCE, Vol. 95, ST12, Dec. 1969, pp. 2687-2701.

[11] G. Grossman, "Analysis of Rim Supports for off-axis inflatable reflectors II – Deformations", Journal of the Aerospace Division, ASCE, vol. 4, Jan. 1991.

[12] A.L. Palisoc and G.C. Pardoen, "A user interface and finite element analysis of inflatable parabolic antennas project summary", L'Garde Technical Report, LTR-93-AP-043, July 1993. G.C. Pardoen developed the FAIM code under a L'Garde project. It was initially called LDIPS.

[13] Femap is an engineering analysis program by Siemens PLM Software, used to build finite element models of engineering problems and for viewing solution results.

[14] N.E. Gibbs, W. G. Poole, Jr and P.K. Stockmeyer, "An algorithm for reducing the bandwidth and profile of a sparse matrix", SIAM J Numer Anal, Vol 13, No. 2, April 1976.

[15] H, Hencky, "Uber den Spannungszustand in kreisrunden Platten mit verschwindender Biegungssteifigkeit", Zeits. Math Phys. Vol. 63, pp. 311-316, 1915.

[16] W.B. Fichter, "Some Solutions for the large deflections of uniformly loaded circular membranes", NASA Technical Paper 3658, Langley Research Center, Hampton, Virginia, July 1997.

[17] A.L. Palisoc and Y. Huang, "Design Tool for Inflatable Space Structures", SDM Conference, AIAA-97-1378, Kissimmee, Florida, 1997.

[18] Timoshenko, S. and Goodier, J.N., "Theory of Elasticity", 2nd edition, McGraw-Hill, New York, 1951.

[19] Johns, D.J., "Thermal Stress Analysis", 1st Edition, Pergamon Press, Oxford, 1963.

[20] Dugdale, D.S., "Elements of Elasticity", 1st Edition, Pergamon Press, Oxford, 1968.

[21] G. Pardoen, "Two-Dimensional Thermoelasticity", unpublished L'Garde Technical Report, May 2021.

[22] A.L. Palisoc and M. Thomas, "A comparison of the performance of seamed and unseamed inflatable concentrators", Solar Engineering, vol. 2, ASME 1995.

[23] Y. Takashima, et al, "All reflective THz telescope design with a 20m inflatable primary antenna for Orbiting Astronomical Satellite for Investigating Stellar Systems (OASIS) mission", Proc SPIE, Optics+Photonics, San Diego, California, 1-5 August 2021

[24] A.L. Palisoc, "Large Inflatable Structures", L'Garde Technical Report, LTR-98-AP-021, June 1998.

[25] G. Poe and B.G. Patrick, "Zero CTE polyimides for athermal optical membranes", Proc. SPIE – The International Society for Optical Engineering, August 2008.